Near-Surface Vortex Intensification through Corner Flow Collapse

D. C. LEWELLEN AND W. S. LEWELLEN

West Virginia University, Morgantown, West Virginia

(Manuscript received 26 April 2006, in final form 23 October 2006)

ABSTRACT

Results are presented from a large set of large-eddy simulations of a class of unsteady vortex evolution that may sometimes play a role in tornadogenesis or tornado variability. Beginning with a high-swirl parent vortex with an excess of low-swirl flow through the surface/corner/core region, perturbation of the low-swirl near-surface inflow at a large radius can trigger a subsequent dynamic "corner flow collapse" producing dramatic near-surface intensification relative to conditions aloft of an order of magnitude or more in velocity scale. This paper presents a more detailed treatment of the physics and simulation of corner flow collapse, expanding upon the presentation given in a companion paper treating near-surface vortex intensification more generally for both steady and unsteady conditions. The basic scaling of the onset, intensification, structure, and duration of the phenomenon is explored as a function of some of the dominant physical parameters involved. A dimensionless rate of change of the low-swirl flux through the surface/corner flow during the process is identified as a critical governing parameter. Given the mode of triggering near the surface at large radii, the large intensification that can result, and the sensitivity to some of the parameters involved, corner flow collapse may provide a mechanism by which the rear-flank downdraft can promote tornadogenesis and help explain why seemingly similar conditions sometimes produce intense tornadoes and other times do not.

1. Introduction

Tornadoes can form rapidly and exhibit markedly strong variations in surface intensity during their lifetimes. We have argued in previous work that much of this variability arises from the sensitivity of the structure and intensity of a vortex corner flow to the low-swirl boundary layer inflow that feeds it. There has been considerable effort spent over the past few decades in trying to understand vortex corner flow structure in the quasi-steady state with the boundary layer developed purely through surface friction. There has been comparatively little systematic work done on time-varying cases, and/or more general configurations of near-surface inflow that might occur. In a companion paper (Lewellen and Lewellen 2007, hereafter LL1) a simplified analytical model and large-eddy simulations were used to explore near-surface intensification of both quasi-steady and unsteady turbulent vortices relative to conditions aloft. It was shown in particular that a class of vortex evolution leading to a dynamic corner flow collapse (CFC) can naturally produce a very intense near-surface vortex from a much weaker larger-scale swirling flow, and it was argued that this might sometimes play a critical role in tornadogenesis and/or tornado variability.

We begin by addressing important simulation concerns in section 2, particularly the grid resolution requirements and interaction with the top boundary condition. We then sample the range of behavior encountered and address what governs the greatest levels of near-surface intensification, its onset, and duration in section 3. In doing so we draw on results from over a hundred high-resolution large-eddy simulations of corner flow collapse, though only a subset are presented in any detail below. We concentrate here on cases for which the evolution is at least roughly axisymmetric, which permits more systematic quantitative analysis of the results. While we have performed many asymmetric corner flow collapse simulations and find the results in basic qualitative agreement with more symmetric cases (cf. LL1, their Fig. 12), we defer systematic discussion of these cases to a future paper. Section 4 concludes

Corresponding author address: D. C. Lewellen, MAE Dept., P.O. Box 6106, West Virginia University, Morgantown, WV 26506-6106.
E-mail: dclewellen@mail.wvu.edu

DOI: 10.1175/JAS3966.1

with a summary and further discussion. A key to the principal simulations referred to in this paper follows in an appendix.

For a presentation of the basic corner flow collapse evolution, discussion of how it achieves large near-surface intensification, definitions, and model description the reader is referred to LL1. It and the present paper more systematically expand upon earlier presentation of the phenomenon (Lewellen et al. 2000b; Lewellen and Lewellen 2002). There are several other examples in the literature of unsteady (generally axisymmetric) simulations leading to transient near-surface intensification (e.g., Walko 1988; Fiedler 1994). Some of these (cf. particularly Davies-Jones 2000; Markowski et al. 2003) exhibit features suggesting that corner flow collapse is likely a contributing ingredient in the process.

2. Simulating corner flow collapse

The large-eddy simulation model used and procedures employed are as described in LL1. Unless otherwise noted, the results presented are nondimensionalized as in LL1 using the far-field angular momentum level (Γ_∞) and the domain "radius" ($r_d \equiv$ half the lateral domain size) to form length (r_d), time ($t_s \equiv r_d^2/\Gamma_\infty$), and velocity ($V_s \equiv \Gamma_\infty/r_d$) scales.

a. Grid resolution

The basic grid requirements for resolving the most important turbulent structures within a quasi-steady vortex corner flow were assessed in Lewellen et al. (1997). New issues arise in simulating a corner flow collapse, however. At the time of peak near-surface intensification, the event can be nearly singular, as shown in LL1.

Figure 1 shows different measures of near-surface intensification versus time for five simulations (A0.5, A1, A2, A4, A8) with differing finest horizontal grid resolution (spanning a factor of 16). The case simulated is the one illustrated in most detail in LL1 (their Figs. 8–11), which exhibits a strong narrow updraft jet off the surface at the time of peak intensity. The peak values obtained are clearly sensitive to the central grid resolution, although this sensitivity is reduced when azimuthally averaged results are considered (e.g., Fig. 1d). An examination of the evolving velocity fields for these cases shows that the sensitivity to grid resolution is essentially confined to the region of the inner updraft jet around the time of peak intensification. The basic corner-flow collapse process otherwise proceeds in identical fashion, with the same corner flow structures encountered, for any of these grid resolutions. For example, Fig. 2 shows results from five different simulations of corner flow collapse at the time of peak intensification. Included are the highest and lowest resolution simulations from Fig. 1 (A0.5 and A8), showing that results on this scale are indistinguishable for all practical purposes. Moreover, for some "less focused" corner-flow collapse scenarios, the grid sensitivity in this resolution range was found to drop out even for the local peak values of intensification.

Except where noted, all of the results presented below are from simulations with the middle resolution in Fig. 1 (0.2% of r_d in the central region). In comparing peak values of velocity and pressure it appears prudent to compare results from simulations with the same fine resolution (or to consider azimuthal averages). For most of our purposes here in illustrating basic features of the phenomenon, however, even more modest resolution seems to suffice: the basic results illustrated below were all reproduced in lower resolution simulations as well.

Because this is a turbulent, unsteady process it is also important to address how quantitatively reproducible the phenomena is for slightly altered initial conditions. Generally, for fixed resolution, the primary features have proved quite reproducible, though secondary variations are evident (particularly after the main intensification peak). Simulation Aa, initialized from the same quasi-steady simulation sampled at a different time, provides an example (Figs. 2e,j and Fig. 3 below).

b. Boundary conditions

In an "open" domain the simulation results are largely governed by the boundary conditions imposed. For corner-flow collapse simulations this includes both the fixed boundary conditions that produced the quasi-steady initial state used and the changes to those conditions used to trigger the time development. Within an actual severe storm the large-scale conditions that would be present outside the simulation domain initially are, of course, not steady state: the assumption invoked is that those external conditions during the prior development change slowly enough relative to the dynamic time scales of the interior flow that the latter keeps in approximate quasi-steady equilibrium with the former. While still an idealization, such starting conditions are more realistic than ones that would not be achieved in nature, even in an approximate sense (e.g., a flow field in uniform solid-body rotation with no vertical velocity).

In a severe storm, coherent changes on large spatial scales require longer times than changes on smaller

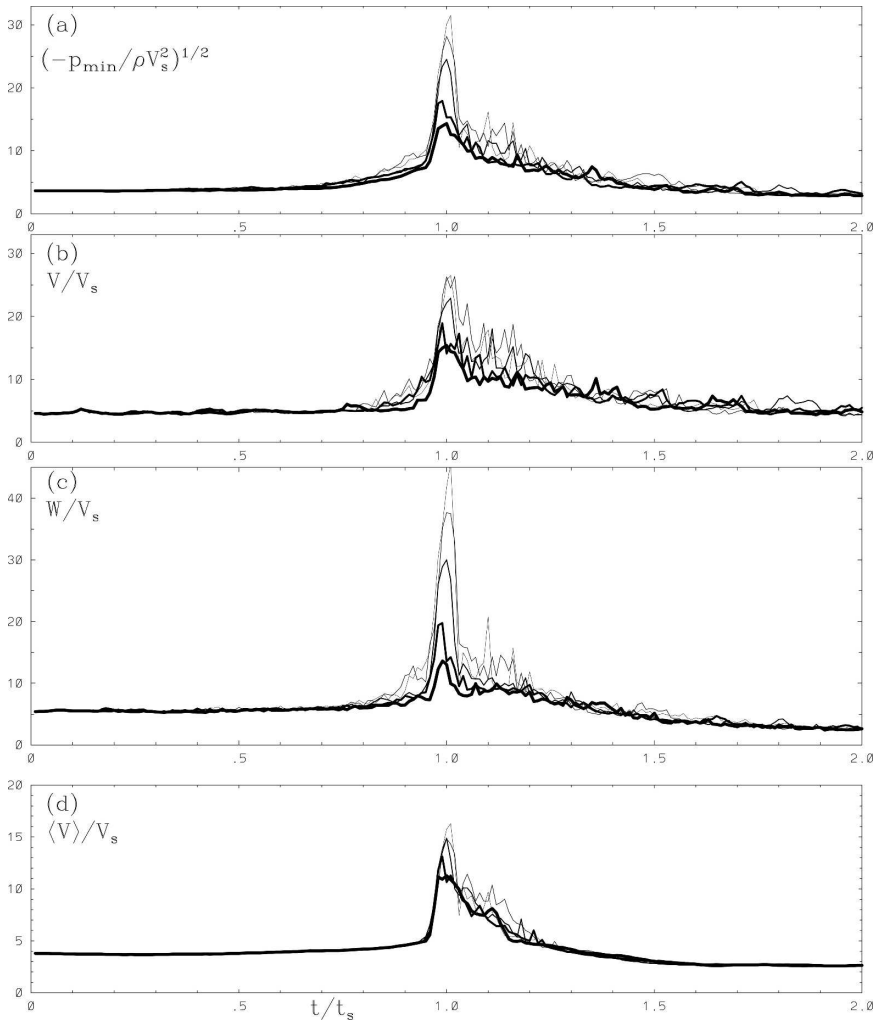

FIG. 1. Nondimensionalized peak (a) square root pressure drop, (b) swirl velocity, (c) vertical velocity, and (d) azimuthally averaged swirl velocity vs time during a corner flow collapse for simulations A8, A4, A2, A1, A0.5 with increasingly refined central horizontal resolution (thick to progressively thinner lines).

scales. Accordingly, in triggering the corner flow collapse simulations, we have not used rapid changes in the overall boundary conditions governing the flow, but restricted the changes to a localized component—the near-surface inflow layer at the outer domain boundary. For the simulations presented here, these changes have been applied around the entire square domain boundary near the surface. Again, this represents a significant idealization. The principal benefit (besides simplicity) is that it keeps the intensifying vortex vertical and centered within the domain to a very good approximation, allowing the angular momentum development to be studied unambiguously and permitting efficient use of the stretched grid spacing employed. In a strongly swirling flow, likely physical mechanisms for impeding the near-surface low-swirl inflow (such as the impingement of a downdraft or collision with some other flow boundary) will "wrap around" the vortex, but not instantaneously. As noted earlier, this tends to give qualitatively similar results but with an intensifying vortex that twists and moves across the surface, complicating both the high-resolution simulation and the analysis of the results. Note that in our idealized treatment the shutoff is not axisymmetric (which would raise even greater concerns about producing an unphysically fine-tuned evolution) but is imposed on the square boundary. This leads to asymmetries and turbulence generation in the inflow, but not such as to significantly tilt, twist, or translate the main vortex as the lower core contracts.

Of potentially greatest concern is the effect of the conditions imposed on the top boundary, which neces-

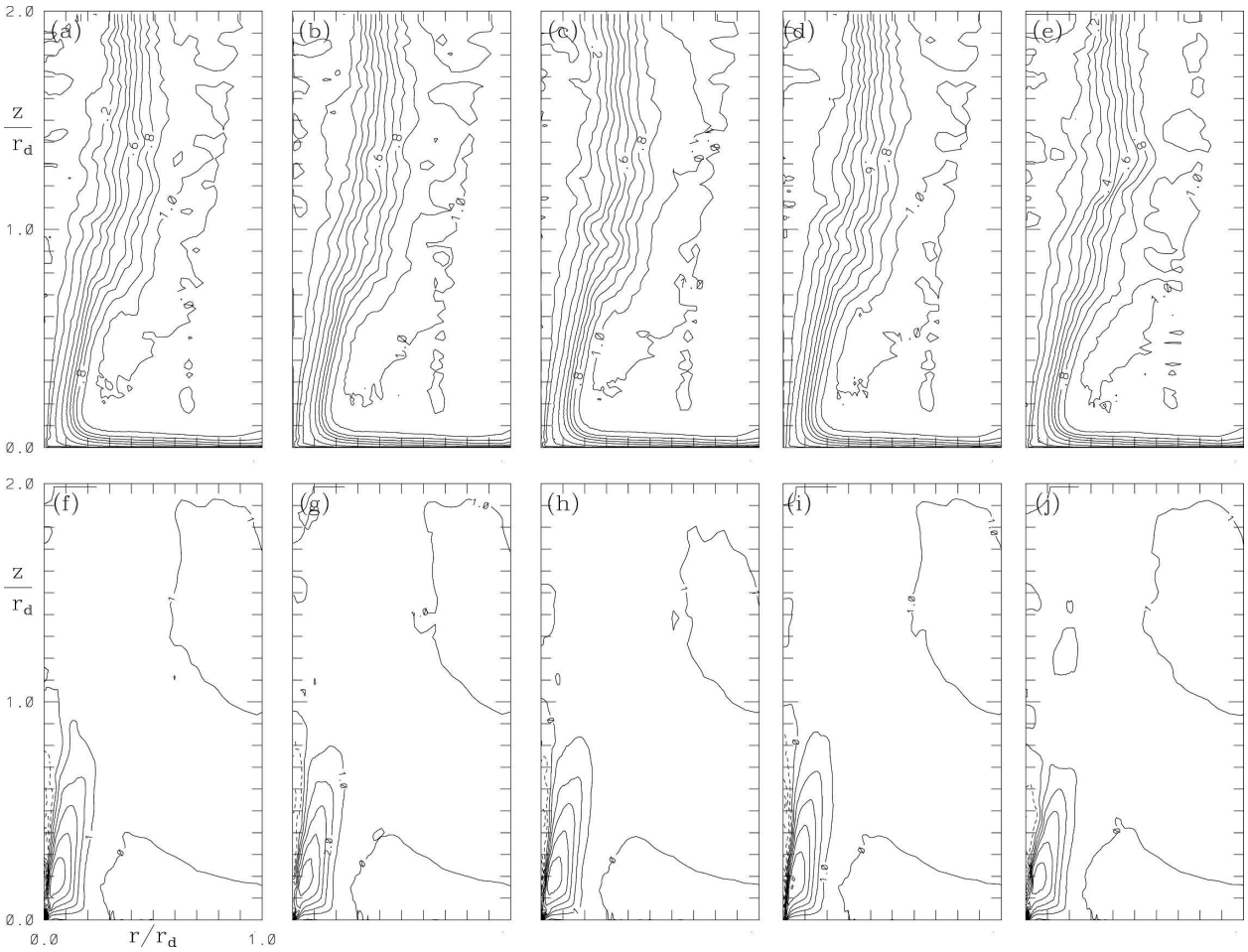

FIG. 2. Azimuthal averages of (top) angular momentum fraction (Γ/Γ_∞) and (bottom) normalized vertical velocity (w/V_s) at the time of peak near-surface intensification for corner flow collapse simulations: (a), (f) A0.5 (very fine central resolution); (b), (g) A8 (coarse central resolution); (c), (h) At (simultaneous top change); (d), (i) Az3 (reduced surface roughness); (e), (j) *Aa* (alternate realization). The contour interval, min and max contours appearing are (a)–(e) (0.1, 0.0, 1.0), (f) (1.0, −4.0, 20.0), (g) (1.0, −2.0, 9.0), (h) (1.0, −3.0, 16.0), (i) (1.0, −4.0, 6.0), and (j) (1.0, −4.0, 14.0).

sarily cuts through the vortex core itself. These conditions certainly affect the initial state of the vortex core, which in turn can affect the corner flow collapse development; this is treated more below. The bigger concern is whether the collapse process would interact in a strong two-way sense with the top boundary, if allowed. For example, if the early stages of the corner flow collapse strongly affected the flow near the top boundary and changes in the flow at the top boundary in turn strongly affected the collapse process, then a physically relevant simulation would require a properly time varying upper boundary condition.

This proves not to be the case. Simulation At provides an example of the relative insensitivity of the corner flow collapse to changes in the upper core during the process (cf. Figs. 2c,h and 3). The simulation is exactly as in A2, but at the initial time when the near-surface low-swirl flow is curtailed the top boundary condition is simultaneously changed from zero vertical velocity over a disk above the core to uniform w on the whole of the top boundary. In the upper part of the domain this change is felt (cf. the change in upper-core pressure in Fig. 3b and in profiles in the upper third of the domain in Figs. 2c,h) and the two simulations will eventually establish quite different new quasi-steady states, but no changes arise within the corner flow during the collapse process (cf. Figs. 3a,c and the lower parts of Figs. 2c,h). Comparison of simulations A2 and Aa (Figs. 2, 3) also provides evidence of this insensitivity since the initial states differ significantly above the large-scale vortex breakdown due to large 3D turbulent fluctuations there. Comparison of simulations F and Fc, discussed below (cf. Figs. 5d,e,i,j, and 10), provides an even more dramatic example, and additional simula-

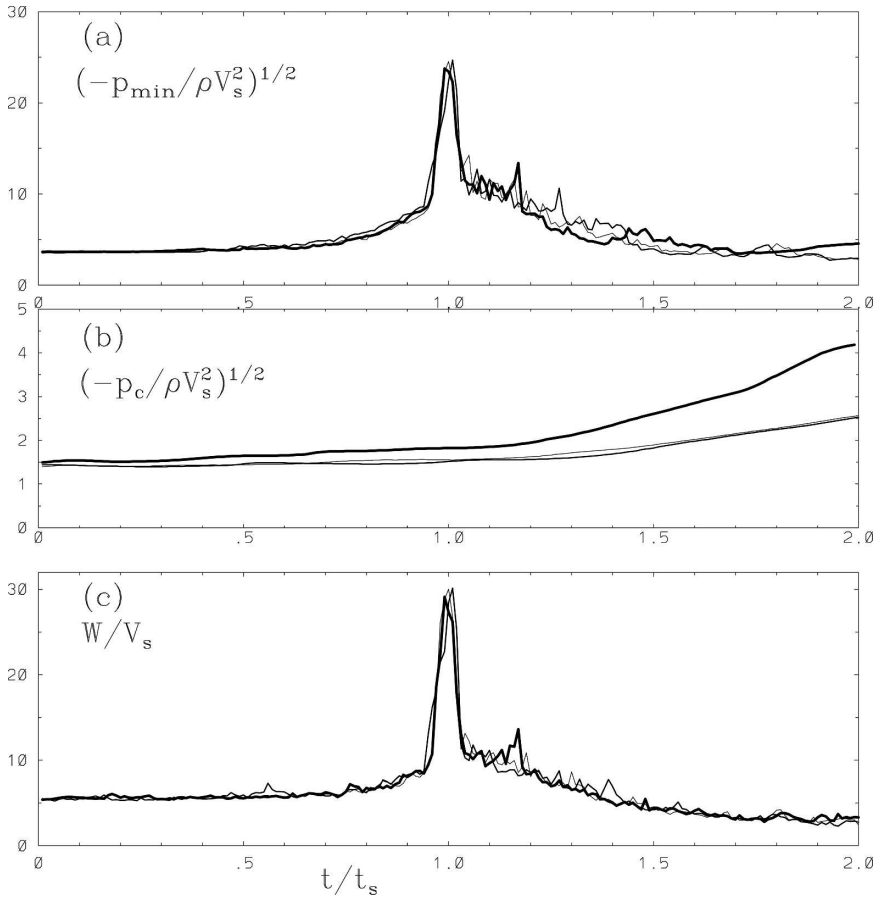

FIG. 3. Nondimensionalized (a) square root peak pressure drop, (b) upper-core pressure drop, and (c) vertical velocity vs time for simulations At (simultaneous top boundary condition change, thick line), A2, and Aa (two realizations, medium and thin lines).

tions that we have performed superposing an upper-core spinup with the CFC support this conclusion as well. The primary reasons for this insensitivity are likely twofold. First, through much of the process the lower core flow is probably supercritical, that is, it lies upstream of a vortex breakdown, and information from above cannot be communicated to the flow below through rotational waves (just as gravitational waves cannot propagate from the downstream side to the upstream side of a hydraulic jump). Second, within the lower corner flow the collapse simply proceeds more rapidly than the larger-scale flow above can adjust in response.

3. Physical variations in CFC

As discussed in LL1, there are several contributing factors to the level of near-surface intensification achieved during a corner flow collapse evolution. We consider now variations of some of these with the aim of obtaining at least rough scaling results for the dominant factors. Figure 4 shows peak azimuthally averaged swirl velocity versus time from three sample sets of corner flow collapse simulations. The three sets differ in their initial conditions, including the domain aspect ratio, upper boundary condition, and near-surface inflow conditions (see the appendix for specifications). Within each set the simulations differ in the rate at which the low-swirl near-surface inflow is reduced. This was achieved in most cases by gradually shutting off the near-surface low-swirl inflow across the lateral boundaries over a specified time rather than abruptly, or (in two of the cases shown) by performing an abrupt shut off at a smaller domain radius. Figure 5 (along with Fig. 2) illustrates some of the azimuthally averaged structure at the time of peak intensification for some of these simulations. We now consider both the basic similarities in these simulations and their differences, particularly in onset time, intensity, structure, and duration.

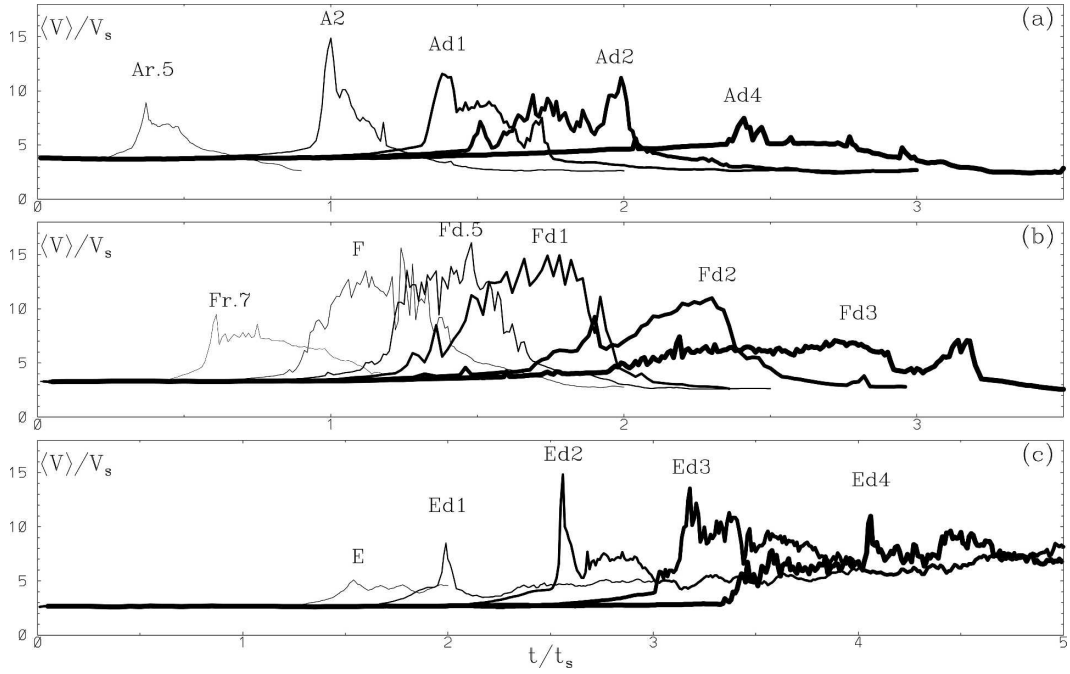

FIG. 4. Nondimensionalized peak azimuthally averaged swirl velocity vs time for sample corner flow collapse simulations, as labeled.

a. Υ *evolution*

CFC can be understood in large part by following the flux of low-swirl fluid passing through the surface-layer, corner, and core flows. For this, we employ the depleted angular momentum flux, Υ, defined as the total flux of the local flow variable $\Gamma_\infty - \Gamma$ (Lewellen et al. 2000a). To good approximation, Υ is a conserved variable (which follows in an incompressible flow from mass and angular momentum conservation) and it has significant value only within the surface/corner/core flow (where $\Gamma < \Gamma_\infty$). Figure 6a summarizes the Υ history within the corner flow for the series of simulations of Fig. 4a. Figure 7 gives a more detailed picture of the Υ development for that case in Fig. 6 that gives the largest intensification: simulation A2. In the quasi-steady initial state Υ is approximately constant (though there is significant large-scale turbulence giving rise to time variation in Υ within the vortex breakdown region in the upper part of the domain). During CFC Υ varies both in time and along the surface/corner/core flow, dropping most rapidly in the surface layer early on with the core catching up only later. The Υ histories plotted in Fig. 6a, $\Upsilon_{c,}$ are those taken within the corner flow itself across a 45° line in the r–z plane that passes through $r = z = 0$ (corresponding to the circles in Fig. 7). There are ambiguities as well in defining the corner flow swirl ratio, $S_c = r_c\Gamma_\infty^2/\Upsilon$, in the evolving case since both the core radius, $r_{c,}$ and Υ depend on where they are measured. For the histories in Fig. 6b the value through the corner is used for Υ and r_c is determined at a height above the surface equal to the initial minimum core size ($0.26r_d$ for this series of runs).

A requirement for the possibility of CFC is that Υ in the initial state is large enough to produce a very low S_c corner flow; that is, one in which the near-surface flow stagnates and lifts off the surface before reaching small radii. As a result, the near-surface velocities (e.g., Fig. 6c) are initially small. The corner flow collapse proceeds by a reduction in Υ so that S_c rises, sweeping through a range of values conducive to large near-surface intensification relative to conditions aloft. While the basic process is robust and reproducible over a wide set of conditions, there is significant variation in the peak intensity, time to reach peak intensity, structure, and duration for different cases (e.g., Figs. 4 and 5). These differences depend in part on the relative magnitudes of different time scales relevant to the CFC process, which we now consider.

b. Time scales for CFC

To proceed, we consider rough scaling estimates for four characteristic time scales: the flow-through time for the large-scale corner flow, t_{TF}; the time for exhausting the low-swirl fluid out of the corner flow from above, t_{exh}; the time window over which S_c takes values conducive to large near-surface intensification, t_{Sc}; and

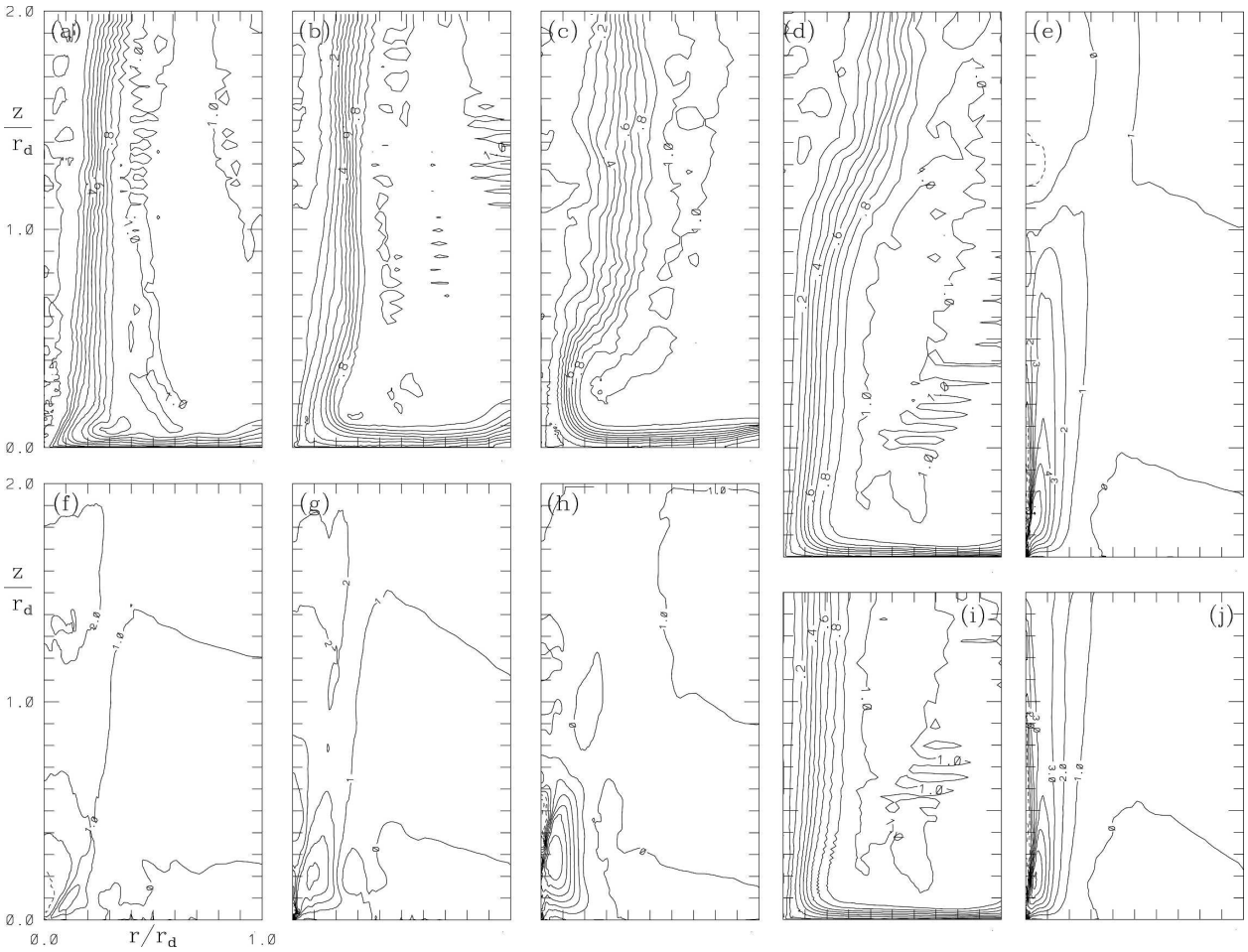

FIG. 5. Azimuthal averages of (a)–(d), (i) angular momentum fraction (Γ/Γ_∞) and (e)–(h), (j) normalized vertical velocity (w/V_s) at the time of peak near-surface intensification for corner flow collapse simulations: (a), (f) E; (b), (g) Ed2; (c), (h) Ad4; (d), (e) F; and (i), (j) Fc. The contour interval and min and max contours appearing are (a)–(d), (i) (0.1, 0.0, 1.0), (e) (1.0, −3.0, 11.0), (f) (1.0, −1.0, 2.0), (g) (1.0, −2.0, 22.0), (h) (1.0, −3.0, 6.0), (j) (1.0, −2.0, 7.0).

the time for exhausting the low-swirl fluid out of the surface layer, t_{surf}. To estimate these the simple model of LL1 is invoked for the initial large-scale corner flow; that is, a zero swirl surface/corner/core flow surrounded by a flow with constant angular momentum Γ_∞. A vortex breakdown is assumed at height Z_b and below it a core flow with radius r_b, vertical velocity $w_b \approx \Gamma_\infty/r_b$, and depleted angular momentum flux $\Upsilon_0 \approx \pi r_b^2 w_b \Gamma_\infty \approx \pi r_b \Gamma_\infty^2$. The domain height is used for Z_b if a vortex breakdown is not present within the domain. The width of the low-swirl peak in S_c space ($\Delta S_c \sim 1$, cf. Fig. 2 of LL1) divided by the time rate of change of S_c around its value at the peak, S_c^*, is used as an estimate for t_{Sc}. Then

$$t_{\text{FT}} \sim \frac{Z_b}{w_b} \sim \frac{Z_b r_b}{\Gamma_\infty} \tag{1}$$

$$t_{\text{exh}} \sim \frac{\text{Volume}}{\text{flux}} \sim \frac{\pi r_b^2 Z_b}{\pi r_b^2 w_b} \sim \frac{Z_b r_b}{\Gamma_\infty} \tag{2}$$

$$t_{Sc} \sim \Delta S_c \Big/ \left(\frac{\partial \Upsilon}{\partial t} \frac{\partial S_c}{\partial \Upsilon}\bigg|_{S_c^*} \right) \sim \frac{r_b \Gamma_\infty^2}{-\partial \Upsilon/\partial t} \frac{\Delta S_c}{S_c^{*2}} \sim \frac{r_b \Gamma_\infty^2}{-\partial \Upsilon/\partial t}. \tag{3}$$

To estimate t_{surf} we assume that the volume of low-swirl fluid in the surface layer, $\mathcal{V}_s$ evolves roughly as

$$\frac{\partial \mathcal{V}_s}{\partial t} \sim \frac{1}{\Gamma_\infty} (\Upsilon_{\text{in}}(t) - \Upsilon_0), \tag{4}$$

where the inflow Υ_{in} is as prescribed for the particular CFC simulation and the outflow into the corner is just taken at its initial value; angular momentum loss to the surface within the domain is neglected in comparison. Equation (4) is integrated for $\mathcal{V}_s(t)$ and t_{surf} is taken as the time for $\mathcal{V}_s$ to reach zero. The initial volume $\mathcal{V}_s(0)$ is required as a boundary condition and estimated as follows. In the quasi-steady initial state the total head is

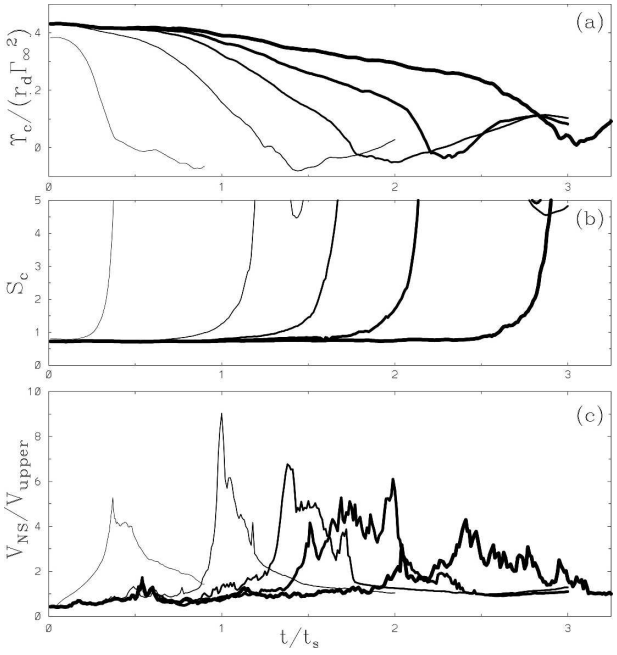

FIG. 6. Time histories for simulations Ar0.5, A2, Ad1, Ad2, Ad4 (thin to thick lines respectively) of (a) normalized depleted angular momentum flux through the corner flow, (b) corner flow swirl ratio, (c) ratio of peak azimuthally averaged near-surface swirl velocity (measured below $0.05r_d$ height) to peak azimuthally averaged swirl velocity in the upper core.

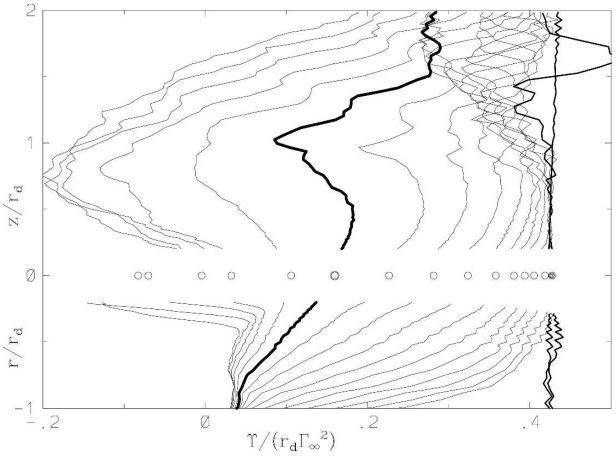

FIG. 7. Depleted angular momentum flux passing sequentially through the surface, corner, and core flow regions for simulation A2 at different times. On the negative y axis are radial profiles of Υ in the surface layer (the integrated flux across vertical planes); on the positive y axis are vertical profiles of Υ up the core (the integrated flux across horizontal planes); and the circles indicate Υ measured within the corner flow (the integrated flux across a 45° plane through $r = z = 0$). The rightmost two profiles (medium thickness) are from the initial quasi-steady state and a time average from that simulation. The other lines represent times $0.1t_s$ apart. The thick line represents Υ at the time of peak intensification.

approximately conserved in the accelerating inflow layer so that the radial velocity $u(r) \sim \Gamma_\infty/r$. Meanwhile $\Upsilon_0 \approx 2\pi u(r)h(r)\Gamma_\infty$ is approximately constant in r, from which we deduce (and find roughly satisfied in simulations) that the surface layer depth is roughly constant, $h \sim \Upsilon_0/(2\pi\Gamma_\infty^2)$. Then, within the square domain, $\mathcal{V}_s(0) \sim 4r_d^2 h \sim 2r_d^2\Upsilon_0/(\pi\Gamma_\infty^2)$. For any prescribed $\Upsilon_{in}(t)$, t_{surf} can be computed; for example, in the simple case of $\Upsilon_{\text{in}} = 0$ for $t > 0$ one finds $t_{\text{surf}} \approx (2r_d^2)/(\pi\Gamma_\infty) = 2t_s/\pi$.

c. Time to peak intensity

Generally we expect the corner flow to collapse and achieve peak intensification when most of the low-swirl fluid has been exhausted from the surface layer and $S_c \approx S_c^* \approx 1.3$. As Fig. 6 indicates, this is at least approximately true for simulations with the largest intensification but, for reasons discussed below, is delayed or advanced somewhat in other cases. The time to reach peak intensity, t_{peak}, depends on the complex coupled surface/corner/core flow dynamics. Nonetheless, it is reasonable to expect t_{peak} to scale with $t_{\text{surf.}}$ Figure 8 supports this expectation.

d. Intensity and structure

Each of the simulations in Fig. 4 exhibits a strong intensification of the vortex near the surface during the corner flow collapse. Also, within each set, the largest velocities are encountered for an intermediate rate of reduction of the low-swirl flux passing through the surface/corner/core flow. This is consistent with the expectations of the model discussed in LL1: a decrease over time in the volume of low-swirl fluid flowing through the corner flow can increase vortex intensity relative to

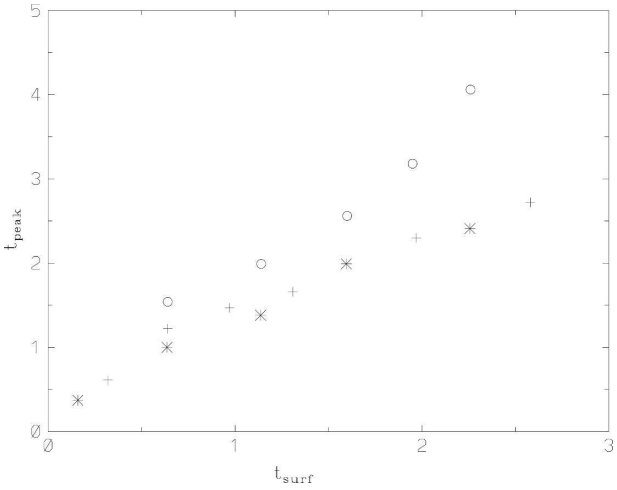

FIG. 8. Time to reach peak intensity, t_{peak}, vs an estimate for the time to exhaust the low-swirl fluid from the surface layer, t_{surf}, for the simulations of Fig. 4; (*) A series, (+) F series, (○) E series.

conditions aloft over and above what can be achieved in a quasi-steady state, but this gain is reduced if the rate of decrease is either too slow or too fast. The LL1 analysis suggests that the most relevant measure of the rate of change of the depleted angular momentum flux through the corner is $(\partial\Upsilon/\partial t)(Z_b/\Gamma_\infty^3) \equiv -\mathcal{R}_\Upsilon$. Figure 9 suggests that $\mathcal{R}_\Upsilon \sim 1$ leads to the largest intensification. In computing $\mathcal{R}_\Upsilon$ for the figure we have taken $\partial\Upsilon/\partial t$ as measured from the simulations during the period before peak intensification when it is nearly constant (cf. Fig. 6a). Using Z_b in formulating the dimensionless measure for the rate of change of Υ improves upon the formulation introduced earlier in Lewellen and Lewellen (2002) using instead the upper-core radius.

1) NEAR OPTIMAL $\partial\Upsilon/\partial T$

For cases with "midrange" levels of $\partial\Upsilon/\partial t$ (i.e., $\mathcal{R}_\Upsilon \sim 1$) leading to the largest near-surface intensification, the structure is generally as described in LL1: a conical form representing nested critical low-swirl corner flows on progressively smaller length scales (cf. Figs. 2 and 5b,d,i). Peak intensification is found when $S_c \approx S_c^*$ (cf. Fig. 6). The Υ development is generally as in Fig. 7, in particular $\Upsilon(z)$ in the lower core is approximately constant at the time of peak intensification, increasing with z before then and decreasing with z afterward. In the analysis of LL1 this gives $\dot{\mathcal{V}} \approx 0$ even with $-\dot{\mathcal{M}}$ large, fostering the unsteady contribution to the near-surface intensification.

2) SMALL $\partial\Upsilon/\partial T$

If Υ varies so slowly that $t_{Sc} \gg t_{FT}$ (i.e., $\mathcal{R}_\Upsilon \ll 1$) then at any time through the evolution the vortex should approximate the structure that it would have in a quasi-steady state; that is, as Υ slowly drops, the corner flow should exhibit structure characteristic of quasi-steady vortices with progressively very-low, low, medium, and high swirl corner flows on the large scale. Qualitatively we find this to be the limit that seems to be approached for the slower developing corner flow collapses: typically a larger scale vortex breakdown descends in the domain and brings a central downdraft to the surface to form a medium-swirl (and eventually high swirl) corner flow structure. This occurs on the large scale before the Υ in the surface layer is reduced sufficiently for an inner corner flow to reach the critical low-swirl point. The nesting of corner flow structures responsible for much of the near-surface intensification in optimal cases is not achieved and the structure at peak intensification (e.g., Figs. 5c,h) is found to be of a more conventional low-swirl type on the larger scale (so at the observed peak $S_c < S_c^*$; cf. simulation Ad4 in Fig. 6).

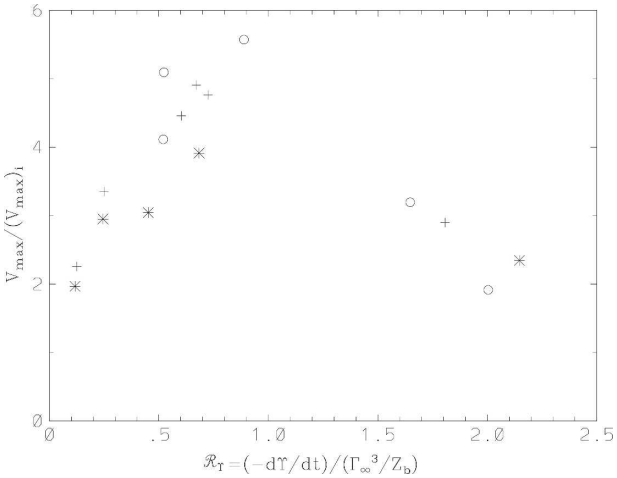

FIG. 9. Ratio of peak azimuthally averaged swirl velocity at the time of peak intensification to its value initially vs $\mathcal{R}_\Upsilon$ for the simulations of Fig. 4 (symbols as in Fig. 8).

3) LARGE $\partial\Upsilon/\partial T$

If, on the opposite extreme, Υ drops so rapidly that $t_{Sc} \ll t_{exh}$ (equivalently $\mathcal{R}_\Upsilon \gg 1$), then S_c sweeps across S_c^* faster than the corner flow can collapse; that is, when the radial overshoot in the near-surface flow is largest, it is prevented from bringing the swirling flow into a central low-swirl jet because the core radius above is still too large. Only the lowest part of the core flow significantly contracts (e.g., Fig. 5a), and the peak intensification then occurs late, for $S_c > S_c^*$ (cf. simulation Ar0.5 in Fig. 6), and is reduced accordingly.

e. Duration

For suitable conditions we expect large near-surface intensification when S_c is in the neighborhood of S_c^*, that is, over a duration $\sim t_{Sc} \sim (r_b\Gamma_\infty^2)(-\partial\Upsilon/\partial t) = (r_b Z_b)/(\mathcal{R}_\Upsilon\Gamma_\infty)$. A compromise is clearly involved in trying to extend the duration of the intensification by reducing $-\partial\Upsilon/\partial t$ since, as discussed above, if $\mathcal{R}_\Upsilon$ is reduced too much, the intensification will fall. On the other hand, for a given velocity level in the core flow prior to CFC (i.e., for fixed Γ_∞/r_b), the duration of the intensification peak can be increased by increasing Z_b. The simulation series in Fig. 4 are in at least qualitative agreement with these scaling predictions, for example, the peak width generally increasing with decreasing $-\partial\Upsilon/\partial t$ and with increasing Z_b (which takes values $\approx 1.2r_d$, $2r_d$, $2r_d$ for run series A, F, and E, respectively), and in rough quantitative agreement for $\mathcal{R}_\Upsilon \sim 1$ (e.g., t_{Sc} is predicted as $0.46t_s$, $0.84t_s$, $0.86t_s$ for simulations A2, F, and Ed2, respectively). Related attempts (not shown) to increase the duration of the intensification peak (or its magni-

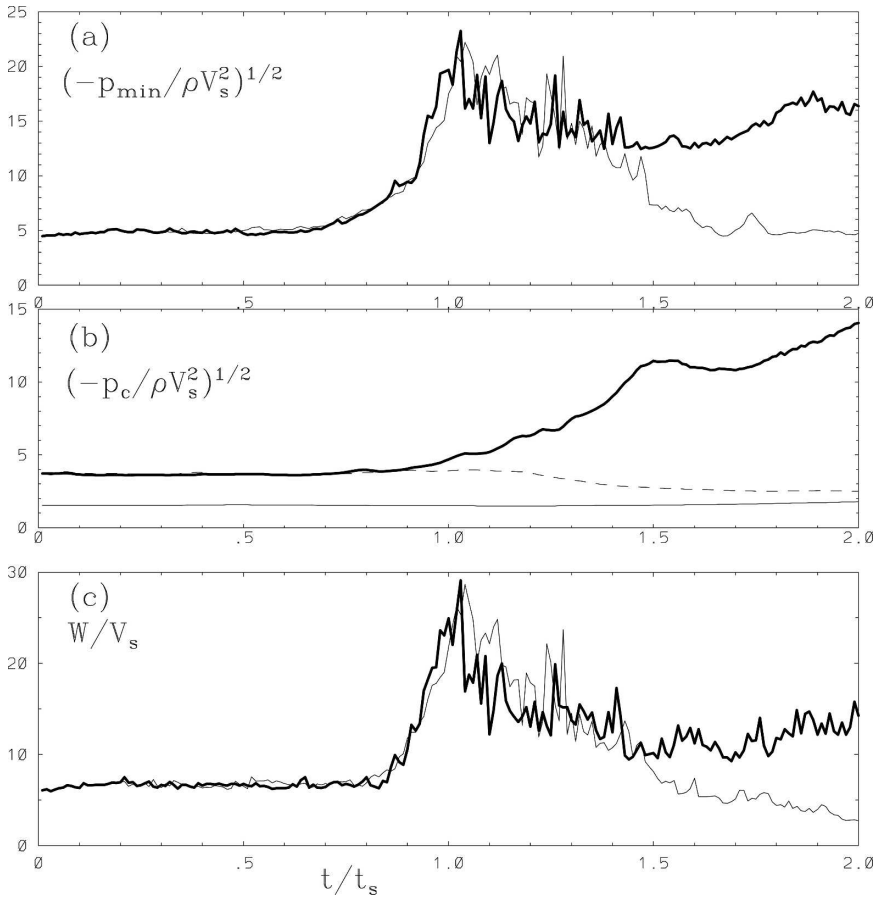

FIG. 10. Nondimensionalized (a) square root peak pressure drop, (b) upper-core pressure drop, and (c) vertical velocity vs time for simulations F (thin lines) and Fc (thick lines). The dashed line in (b) is from the core pressure from simulation F measured at the same height as the upper-core pressure drop from Fc [thick line, (b)].

tude) in other simulations by either forcing a gradual spinup of the upper core during the CFC (by increasing the imposed horizontal convergence) or by adding buoyant forcing from latent heating within the funnel cloud (for tornado-scale simulations) have so far proved relatively ineffectual.

f. Presence or absence of a large-scale vortex breakdown

The A and F series of simulations in Figs. 4a,b include a large-scale vortex breakdown within the domain in the initial state. The E series of Fig. 4c does not. Does this alter the simulation of the CFC in a fundamental way? We address this question directly in comparing simulations F and Fc. The initial state and shutoff of the near-surface inflow for the two simulations is the same, but in Fc the simulation domain is chopped just below the height of the large-scale vortex breakdown in F and the vertical velocity there held in its initial state. A comparison of the two flow fields shows that they evolve essentially in parallel through the time of peak intensification (cf. Figs. 5d,e versus 5i,j). In particular, the narrow central downdraft, whose arrival at the surface cuts off the peak intensification, forms internally in the same way in both simulations, independent of the vortex breakdown above. The two solutions diverge only later as a large-scale downdraft descends from the vortex breakdown in F. Significant differences appear in the lower corner flow only well after the time of peak intensity (cf. Fig. 10). Because of the radically different upper boundary conditions, the two cases eventually head to new quasi-steady states that are vastly different (with the upper core spinning up tightly in one case but not the other). The large pressure drops at later times in Fc seen in Fig. 10a are no longer indicative of extreme near-surface intensification, but of the core pressure having been reduced at

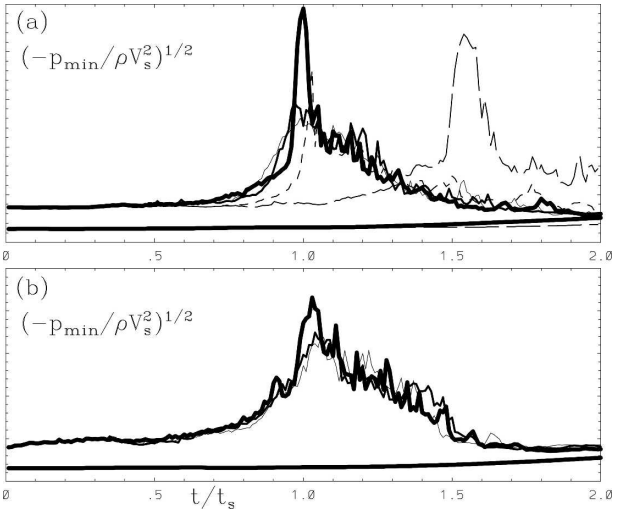

FIG. 11. Nondimensionalized square root peak pressure drop vs time for (a) simulations Az3 (very small z_0, thin solid line), Az2 (small z_0, medium solid line), A2 (default z_0, thick solid), As (swirl reintroduced, short dash), Asd1 (swirl gradually reintroduced, long dash); (b) simulations Bz3 (very small z_0, thin), Bz2 (small z_0, medium), B (default z_0, thick). The nearly flat lines at the bottom of (a) and (b) are from the respective upper-core pressure drops.

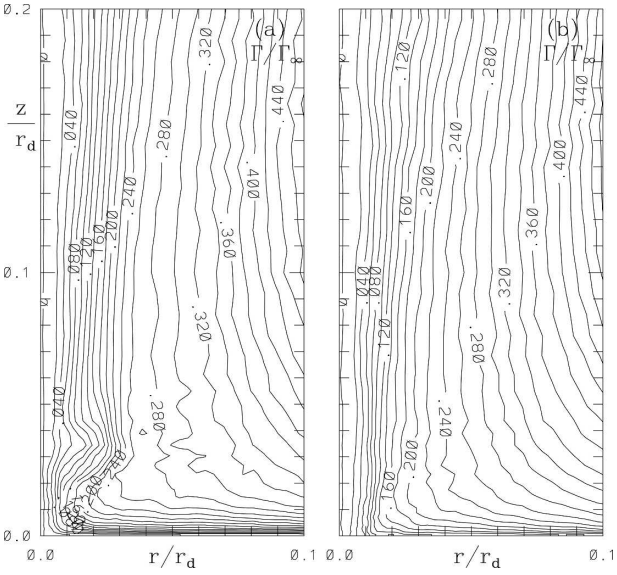

FIG. 12. Contours of azimuthally averaged angular momentum fraction Γ/Γ_∞ for simulations (a) A2 and (b) Az3 at the time of peak intensification.

all heights (cf. Fig. 10b). This is true of the late time behavior of the series E simulations of Fig. 4c as well.

g. Dependence on near-surface inflow structure

The results already shown clearly indicate that the basic large-scale CFC evolution depends on the depleted angular momentum flux and its evolution in the near-surface layer. We now consider the effects of more subtle differences in how Υ is distributed or shut off. Figure 11 shows results from sample runs for which the initial Υ is the same (to within 5%) and the CFC is (with the exception of Asd1) triggered by abruptly shutting off Υ in the inflow at $t = 0$. The cases differ in the choices of surface roughness length (z_0), how the initial low-swirl inflow is distributed and how it is shut off.

Consider first the z_0 dependence in the A series simulations. The largest difference is between A2 and Az2 where an order of magnitude reduction in z_0 produces a factor ~2 reduction in peak velocity scale. A further order of magnitude reduction in z_0 has negligible additional effect (Az3). A detailed comparison of flow field evolution in A2 and Az3 shows that the development on larger length scales is nearly indistinguishable in the two cases (cf. Figs. 2a,f and 2d,i). The differences are confined to the inner corner flow around the time of peak intensification (Fig. 12). As noted in LL1, an important contributing factor to the near-surface intensification achieved during CFC is the realization of nested low-swirl corner flows on different scales. By altering the angular momentum transport to the surface in the lowest layers of the flow, a significant change in z_0 can possibly alter the inner corner flow behavior significantly. For example, a lower z_0 generally reduces angular momentum loss to the surface, thereby decreasing the depleted angular momentum flux near the surface, perhaps enough to change the inner corner flow at the time of peak intensification from a low-swirl to a medium-swirl configuration (e.g., Fig. 12).

Figure 11b indicates that the sensitivity to z_0 is not always large, however. In this series of simulations the near-surface low-swirl inflow in the initial state at the domain boundaries was distributed with angular momentum level increasing linearly from the surface. Compared with the A series simulations this produces an initial state with essentially the same integrated depleted angular momentum flux through the surface/corner/core flow but with different angular momentum gradients and a modestly higher (~25%) vortex breakdown height. Comparison of the flow structure during the CFC in the A and B series simulations (not shown) indicates that the evolution is basically the same in these cases with similar onset times, intensification, and duration. Nonetheless, consistent with the changes in Γ distribution in the surface layer there are some differences encountered in the inner corner flow, including the reduced sensitivity to z_0 evident in Fig. 11.

In simulation As (short dashed line in Fig. 11) Υ at the outer boundary was shut off abruptly by restoring

the far-field angular momentum level, Γ_∞, to the near-surface inflow rather than by shutting off the near-surface inflow itself. As a result the intensity and duration are reduced somewhat. One of the consequences of shutting off Υ by adding swirl is the creation of a body of higher swirl fluid in the surface layer that progresses radially inward. Relative to simulation A2 this produces a modest increase in $\mathcal{R}_\Upsilon$ prior to peak CFC. The observed structure during the collapse (not shown) suggests that the reduction in intensity is due to this increase in $\mathcal{R}_\Upsilon$. The results of simulation Asd1 (long dash, Fig. 11) are consistent with this interpretation: introducing the swirl gradually in time leads to both a decrease in $\mathcal{R}_\Upsilon$ and to increased intensity. Ultimately what is most critical in the CFC process is the restriction of the low-swirl inflow that feeds the vortex core; it is not critical whether the higher swirl flow that replaces it originates from above or enters along the surface.

h. Possible effects of compressibility or debris on peak velocities

The analytical modeling in LL1 (cf. their Fig. A1) and variations with grid resolution of Fig. 1 suggest that, at least in some cases, CFC can be a nearly singular process. It is important, then, to be aware of other physical effects not included in the simulations that may ultimately limit the peak intensification that can be reached. It is clear from Fig. 1 that CFC on the tornado scale could produce significant Mach numbers. Work with a compressible version of the LES code has shown that compressible Mach number effects tend to be modest and may be estimated by an appropriate isentropic transformation applied to the incompressible results (Xia 2001; Xia et al. 2003). This approximation leaves the velocity field unchanged and the reduced density yields an estimate of the reduction in pressure drop within the tornado. Compressible simulations of a corner flow collapse [e.g., Fig. 4 from Xia et al. (2003) showing a compressible version of simulation B here] proved qualitatively very similar to the incompressible ones. The peak pressure drops were reduced by compressible effects at the level predicted by the isentropic transformation, while the peak velocities actually increased somewhat. Compressibility proved no impediment to achieving transonic velocities, supporting earlier compressible axisymmetric results of Fiedler (1997).

It is to be expected that the larger the near-surface velocities the larger the mass of dirt/debris that might be entrained, which in turn might constrain the achievable velocities. Results of a preliminary simulation of corner flow collapse on the tornado scale including small-scale debris showed peak velocities reduced by a third (Lewellen et al. 2004). A key issue appears to be the degree to which the presence of significant debris loading reduces the likelihood of achieving a supercritical end-wall vortex in the inner corner flow.

4. Summary and discussion

In this work sample results from a large set of large-eddy simulations of evolving vortices have been presented to illustrate the basic phenomena, scaling behavior, and variations involved in a particular class of vortex evolutions. Beginning with a larger-scale high-swirl vortex that has a low-swirl surface/corner/core flow (producing a large-scale supercritical end-wall vortex), any impedance of the low-swirl near-surface inflow at large radius (e.g., by shutting off all or part of the inflow or adding swirl to that inflow) can trigger a dynamic corner flow collapse at a later time. This process provides a robust mechanism for creating dramatic intensification of near-surface velocities relative to conditions aloft (up to an order of magnitude or more). Almost all cases simulated have produced significant intensification; however, different conditions lead to large variations in onset time, intensity, corner flow structure, and duration. We have tried to identify some of the dominant scaling behavior in this work, though the number of parameters involved in the actual phenomena preclude a comprehensive quantitative treatment at this point. The most critical parameters are the evolving corner flow swirl ratio, S_c (which must evolve from below $S_c^* \approx 1.3$ to above during the process) and the dimensionless rate of change of the depleted angular momentum flux through the corner flow, $\mathcal{R}_\Upsilon \equiv (-\partial\Upsilon/\partial t)(Z_b/\Gamma_\infty^3)$. The peak intensification is reduced and the corner flow structure altered if $\mathcal{R}_\Upsilon$ is either much greater or much less than $\sim$1. The time between perturbing the near-surface inflow and achieving peak intensification scales with the time required to exhaust the low-swirl fluid out of the surface layer; in the simplest case of a sudden shut off, this scales with the square of the shutoff radius divided by the angular momentum level (Γ_∞) of the vortex aloft. Beginning with a large-scale supercritical vortex of radius r_b and depth Z_b the duration of large intensification during corner flow collapse was predicted to scale as $\sim r_b Z_b/(\mathcal{R}_\Upsilon \Gamma_\infty)$. In addition, the initial structure of the upper vortex core and near-surface inflow, the surface roughness, and how the low-swirl near-surface inflow was reduced were found to be of secondary importance.

Corner flow collapse is an attractive possible pathway for naturally achieving an intense near-surface vortex from a much larger-scale less intense swirling flow.

Applied on the mesocyclone scale, it is a possible route by which the rear-flank downdraft (RFD), by perturbing the low-level inflow, could promote tornadogenesis. In this scenario whether a strong tornado (or any) actually occurs and its duration may depend on the state of the mesocyclone when the downdraft reaches the surface, the radius at which the downdraft is located, its strength or extent, or how rapidly or completely it wraps around the mesocyclone center (since these can affect the dimensionless rate of change of the flux of low-swirl fluid into the corner flow region). This sensitivity might explain why some mesocyclones produce tornadoes while other similar ones do not (Wakimoto and Cai 2000). It also provides an alternate possible mechanism to that proposed in Markowski et al. (2003) for the apparent correlation of tornado occurrence/intensity and surface RFD thermodynamic properties (Markowski et al. 2002). Markowski et al. (2003) attribute this correlation to direct buoyancy forcing effects, based on axisymmetric simulation experiments (some of which show structure strongly suggestive of CFC, e.g., their experiment 1; Figs. 6–8). The CFC results here show as well that for a dramatic vortex intensification it is not required that the angular momentum brought to the surface by the downdraft be forced toward the vortex center (as in Davies-Jones 2000; Markowski et al. 2003): it is enough if the near-surface low-swirl inflow is sufficiently impeded, whereupon high angular momentum fluid from above will automatically be drawn down from above to replace it.

Several caveats are in order in interpreting the present results on the mesocyclone scale, however. Deviations from approximate axisymmetry will be significant on this scale. Buoyancy effects, neglected here, will likely significantly modify the process on this scale, particularly affecting the initial state (e.g., how the initial large-scale vortex is capped) and the dynamics of large-scale core downdrafts later on (likely extending tornado duration). In any case, we are not suggesting CFC as a unique mechanism for tornadogenesis, or always a contributing factor, but likely one of many. Indeed, we have encountered possible alternatives within our simulations. For example, for some conditions, "unfavorable" levels of $\mathcal{R}_\Upsilon \ll 1$ leading to partial corner flow collapse forcing a strong central downdraft were found to produce one or more intense transient vortices in the resulting annular shear layer. This is similar to the interpretation of the Garden City tornadogenesis given in Wakimoto and Liu (1998).

On the tornado scale, CFC provides an additional mechanism contributing to the high degree of variability encountered in tornado intensity and corner flow structure encountered during their lifetimes [as evidenced, e.g., in damage tracks or with Doppler radar (Wurman and Alexander 2005)]. While the simulations presented here illustrated basic scenarios of single CFC events, more varied changes in the inflow at large radius (e.g., cyclically reducing and increasing the low-swirl inflow in one quadrant) could lead to correspondingly varied histories, including low-swirl intensification spikes, periods with multiple secondary vortices, and gaps in damage paths. Simulating such cases (particularly with the inclusion of debris and simulated damage tracks) is one possibility for future research in this area.

Other priorities for extending this research include a systematic treatment of asymmetric corner flow collapse, a more complete categorization of which initial conditions are (or are not) susceptible to developing large near-surface intensification, and what flow changes can (or cannot) trigger that development. The sensitivity of tornado occurrence and intensity to the near-surface flow in the CFC scenarios (among others) suggests that predicting tornado occurrence based on accessible radar measurements of large-scale features probably has inherent uncertainties. Nonetheless, it may still be possible to rule out tornado occurrence based on those measurements for some (possibly large) classes of conditions. Finally, as more complete observations of developing wind fields in tornadic storms become available (particularly near the surface), it will be important to try to identify observational evidence for corner flow collapse on different scales. It could prove interesting and fruitful to realize the basic phenomena in laboratory tornado models as well.

Acknowledgments. This work was supported by National Science Foundation Grant ATM236667.

APPENDIX

Principal Simulations

The corner flow collapse simulations are separated into run series based on the boundary conditions of the quasi-steady simulations used for initial conditions. Those used for the figures in the present work are listed in Table A1. The conditions are nondimensionalized using the far-field angular momentum level (Γ_∞) and the domain radius ($r_d \equiv$ half the lateral domain size) to form length (r_d), time ($t_s \equiv r_d^2/\Gamma_\infty$), and velocity ($V_s \equiv \Gamma_\infty/r_d$) scales. As examples a dimensionalization on the tornado scale could be $\Gamma_\infty = 10^4$ m^2 s^{-1} and $r_d = 1$ km giving $t_s = 100$ s and $V_s = 10$ m s^{-1}; or, on the mesocyclone scale, $\Gamma_\infty = 4 \times 10^4$ m^2 s^{-1} and $r_d = 5$ km produce $t_s = 625$ s and $V_s = 8$ m s^{-1}.

For a given set of initial conditions, several simulations were generated: for example by varying the finest

TABLE A1. Conditions for the principal simulation series considered in the text. Here $a_c^{\text{lateral}}(z)$ and $\Gamma^{\text{lateral}}(z)$ are the vertical profiles of the horizontal convergence and angular momentum at the side boundaries, respectively. Two constant values for the vertical velocity on the top boundary are specified in each case: w_c^{top} within a core disk of radius $0.25r_d$ and w_U over the remainder, with the sum set to satisfy mass continuity. All have horizontal × vertical domain sizes of $2r_d \times 2r_d$ except *F* with $2r_d \times 3r_d$ and finest vertical grid spacing (located at the surface) of $10^{-3}r_d$.

Series	$a_c^{\text{lateral}}(z)r_d^2/\Gamma_\infty$	$\Gamma^{\text{lateral}}(z)/\Gamma_\infty$	$w_c^{\text{top}}r_d/\Gamma_\infty$	Evolution trigger
A	1.0 for $z < r_d$ 0.0 for $z > r_d$	0 for $z < 0.1r_d$ 1 for $z > 0.1r_d$	0	Inflow shut off below $z = 0.1r_d$
B	1.0 for $z < r_d$ 0.0 for $z > r_d$	$z/(0.2r_d)$ for $z < 0.2r_d$ 1 for $z > 0.2r_d$	0	Inflow shut off below $0.2r_d$
E	1.0 for $z < r_d$ 0.0 for $z > r_d$	0 for $z < 0.2r_d$ 1 for $z > 0.2r_d$	w_U	Inflow shut off below $z = 0.2r_d$
F	1.0 for $z < 0.2r_d$ $(2.5 - z/r_d)/2.3$ for $0.2 < z/r_d < 2.5$ 0.0 for $z > 2.5r_d$	$z/(0.2r_d)$ for $z < 0.2r_d$ 1 for $z > 0.2r_d$	−0.8	Inflow shut off below $0.2r_d$

horizontal grid resolution (Δx, located in the center of the domain), the surface roughness length (z_0), time over which the near-surface inflow layer was shut off to trigger the corner flow collapse (t_{off}), etc., as listed below. Unless otherwise noted default values of $\Delta x/r_d = 2 \times 10^{-3}$, $z_0/r_d = 2 \times 10^{-4}$, and $t_{\text{off}} = 0$ were used.

- A series: (shallow no-swirl inflow layer near surface)
- resolution: A0.5, A1, A2, A4, A8 ($10^3\Delta x/r_d = 0.5$, 1, 2, 4, 8, respectively)
- roughness: Az2, Az3 ($z_0/r_d = 2 \times 10^{-5}$, 2×10^{-6})
- shut off: Ad1, Ad2, Ad4 ($t_{\text{off}}\Gamma_\infty/r_d^2 = 1$, 2, 4, respectively), Ar0.5 (shut off at $0.5r_d$), As (inflow switched to $\Gamma = \Gamma_\infty$ below $z = 0.1r_d$), Asd1 (as in As but switched gradually over time r_d^2/Γ_∞)
- other: At (top boundary condition switched to uniform outflow at $t = 0$), Aa (alternate realization of A2)
- B series: (inflow Γ rising linearly near surface) roughness B, Bz2, Bz3 ($z_0/r_d = 2 \times 10^{-4}$, 2×10^{-5}, 2×10^{-6}, respectively)
- E series: (no large-scale vortex breakdown; thicker no-swirl inflow layer)
- shut off: E, Ed1, Ed2, Ed3, Ed4 ($t_{\text{off}}\Gamma_\infty/r_d^2 = 0$, 1, 2, 3, 4, respectively)
- F series: (deeper domain; inflow Γ rising linearly near surface)
- shut off: F, Fd0.5, Fd1, Fd2, Fd3 ($t_{\text{off}}\Gamma_\infty/r_d^2 = 0$, 0.5, 1, 2, 3, respectively), Fr0.7 (shut off at $0.707r_d$)
- other: Fc (as in F but domain reduced to $1.5r_d$ height with the initial vertical velocity distribution held steady as the top boundary condition).

Many other simulations were performed over the course of this study, often at coarser horizontal resolution. Parameters varied included the domain dimensions, horizontal convergence, angular momentum distributions, top boundary conditions, surface roughness, and initial S_c, Υ, Z_b, and surface layer depth. Modes of triggering corner flow collapse included abrupt shut off of the low-swirl near-surface inflow at the outer domain boundary, gradual shut off, shut off over part of the boundary or a sequential shut off around the boundary, shutting off only part of the low-swirl inflow, reintroducing swirl to the low-level inflow, or switching the low-level inflow abruptly to outflow. A representative sample of the better resolved and more complete run series were selected for inclusion here to best illustrate general results from the larger set.

REFERENCES

Davies-Jones, R., 2000: Can the hook echo instigate tornadogenesis barotropically? Preprints, *20th Conf. on Severe Local Storms,* Orlando, FL, Amer. Meteor. Soc., 269–272.

Fiedler, B. H., 1994: The thermodynamic speed limit and its violation in axisymmetric numerical simulations of tornado-like vortices. *Atmos.–Ocean,* **32,** 335–359.

——, 1997: Compressibility and windspeed limits in tornadoes. *Atmos.–Ocean,* **35,** 93–107.

Lewellen, D. C., and W. S. Lewellen, 2002: Near-surface intensification during unsteady tornado evolution. Preprints, *21st Conf. on Severe Local Storms,* San Antonio, TX, Amer. Meteor. Soc., CD-ROM, 12.8.

——, and ——, 2007: Near-surface intensification of tornado vortices. *J. Atmos. Sci.,* **64,** 2176–2194.

——, ——, and J. Xia, 2000a: The influence of a local swirl ratio on tornado intensification near the surface. *J. Atmos. Sci.,* **57,** 527–544.

——, ——, and ——, 2000b: Nonaxisymmetric, unsteady tornadic corner flows. Preprints, *20th Conf. on Severe Local Storms,* Orlando, FL, Amer. Meteor. Soc., 265–268.

——, B. Gong, and W. S. Lewellen, 2004: Effects of debris on near-surface tornado dynamics. Preprints, *22d Conf. on Se-*

vere Local Storms, Hyannis, MA, Amer. Meteor. Soc., CD-ROM, 15.5.

Lewellen, W. S., D. C. Lewellen, and R. I. Sykes, 1997: Large-eddy simulation of a tornado's interaction with the surface. *J. Atmos. Sci.,* **54,** 581–605.

Markowski, P. M., J. M. Straka, and E. N. Rasmussen, 2002: Direct surface thermodynamic observations within the rear-flank downdrafts of nontornadic and tornadic supercells. *Mon. Wea. Rev.,* **130,** 1692–1721.

——, ——, and ——, 2003: Tornadogenesis resulting from the transport of circulation by a downdraft: Idealized numerical simulations. *J. Atmos. Sci.,* **60,** 795–823.

Wakimoto, R. M., and C. Liu, 1998: The Garden City, Kansas, storm during VORTEX 95. Part II: The wall cloud and tornado. *Mon. Wea. Rev.,* **126,** 393–408.

——, and H. Cai, 2000: Analysis of a nontornadic storm during VORTEX 95. *Mon. Wea. Rev.,* **128,** 565–592.

Walko, R. L., 1988: Plausibility of substantial dry adiabatic subsidence in a tornado core. *J. Atmos. Sci.,* **45,** 2251–2267.

Wurman, J., and C. R. Alexander, 2005: The 30 May 1998 Spencer, South Dakota, storm. Part II: Comparison of observed damage and radar-derived winds in tornadoes. *Mon. Wea. Rev.,* **133,** 97–119.

Xia, J., 2001: Large-eddy simulation of a three-dimensional, compressible tornado vortex. Ph.D. thesis, West Virginia University, 150 pp. [Available online at http://etd.wvu.edu/templates/showETD.cfm?recnum=2216.]

——, W. S. Lewellen, and D. C. Lewellen, 2003: Influence of Mach number on tornado corner flow dynamics. *J. Atmos. Sci.,* **60,** 2820–2825.